Syntheses, Structures, and Properties of Six Novel Alkali Metal Tin Sulfides: $K_2Sn_2S_8$, α-$Rb_2Sn_2S_8$, β-$Rb_2Sn_2S_8$, $K_2Sn_2S_5$, $Cs_2Sn_2S_6$, and Cs_2SnS_{14}

Ju-Hsiou Liao, Constantinos Varotsis, and Mercouri G. Kanatzidis*

Department of Chemistry and Center for Fundamental Materials Research, Michigan State University, East Lansing, Michigan 48824

Received October 8, 1992

Six alkali metal tin polysulfides and one monosulfide, $K_2Sn_2S_8$ (I), α-$Rb_2Sn_2S_8$ (II), β-$Rb_2Sn_2S_8$ (III), $K_2Sn_2S_5$ (IV), $Cs_2Sn_2S_6$ (V), and Cs_2SnS_{14} (VI), respectively, were synthesized by a molten salt technique. I and IV were made by heating mixtures of Sn/K_2S/S (molar ratio 1/2/8) at 275 and 320 °C, respectively, for 4–6 days. II and III were made by heating mixtures of Sn/Rb_2S/S (molar ratio 1/2/12 for II and 1/1/8 for III at 330 and 450 °C, respectively, for 4–6 days. V and VI were made by heating mixtures of Sn/Cs_2S/S (molar ratio 1/3/8 for V and 1/2/8–12 for VI at 275 °C for 4–6 days. The crystals form in a K_2S_x, Rb_2S_x, and Cs_2S_x flux, respectively. Orange crystals of I crystallize in the monoclinic space group $P2_1/n$ with a = 9.580(8) Å, b = 10.004(5) Å, c = 14.131(7) Å, β = 107.82(6)°, and Z = 4. Orange crystals of II and III have the same anionic frameworks as I. II crystallizes also in the monoclinic space group $P2_1/n$ with a = 9.788(3) Å, b = 9.978(3) Å, c = 14.360(2) Å, and β = 106.70(2)°, and Z = 4. III crystallizes in the orthorhombic space group $Pbcn$ with a = 9.987(5) Å, b = 19.635(3) Å, c = 13.747(3) Å, and Z = 8. The yellow-orange IV crystallizes in the monoclinic space group $C2/c$ with a = 11.804(3) Å, b = 7.808(1) Å, c = 11.539(1) Å, β = 108.35(1)°, and Z = 4. The yellow V crystallizes in the triclinic space group $P\bar{1}$ with a = 7.289(4) Å, b = 7.597(3) Å, c = 6.796(3) Å, α = 114.80(3)°, β = 108.56(4)°, γ = 97.54(4)°, and Z = 1. Red crystals of VI are monoclinic, space group $P2_1/n$, with a = 6.964(6) Å, b = 18.66(1) Å, c = 14.80(1) Å, β = 99.39(1)°, and Z = 4. The structures of these six compounds have been determined by single-crystal X-ray diffraction analysis. IR and Raman spectra for these compounds are reported. I–III have novel two-dimensional structures. Each $[Sn_2S_8]_n^{2n-}$ layer is composed of $[Sn_2S_4]_n$ parallel chains, which contain octahedral SnS_6 and tetrahedral SnS_4, cross-linked by S_4^{2-} ligands. Charge-compensating potassium or rubidium cations are found between the layers. IV has the $Tl_2Sn_2S_5$ structure type and has a three-dimensional structure, with $[SnS_3]_n^{2n-}$ chains formed by distorted SnS_5 trigonal bipyramids sharing two of their common edges with one another. Those chains are then cross-linked by sharing the remaining vertices of the trigonal bipyramids to generate parallel tunnels in which potassium cations are located. The structure of V is closely related to IV. It also comprises $[SnS_3]_n^{2n-}$ chains which in a different fashion are cross-linked by S_2^{2-} to form an extended two-dimensional structure. VI contains a molecular $[SnS_{14}]^{2-}$ complex anion with octahedral Sn^{4+} ligated by two S_4^{2-} and one S_6^{2-} chelating ligands. The UV/vis optical properties of I–V are reported. The optical band gaps are 2.15 eV for I–III, 2.36 eV for IV, and 2.44 eV for V.

Introduction

Synthesis of new chalcogenide solids can be achieved at intermediate temperatures (200–450 °C) using the molten salt (flux) method. The latter has been proven to be a successful technique in stabilizing and crystallizing interesting new chalcogenides with novel structure types. In recent years, a series of polychalcogenide compounds synthesized by molten salts using intermediate temperatures have been reported including $K_4Ti_3S_{14}$,[1,2] α-$KCuS_4$, β-$KCuS_4$,[3,4] Na_3AuSe_8,[3] $NaAuSe_2$, $KAuSe_2$,[18] $KAuSe_5$,[3] K_3AuSe_{13},[3,6] $K_2Hg_3Q_4$ (Q = S, Se), $K_2Hg_6S_7$,[3,7] and $K_2Cu_5Te_5$.[8] The versatility of polychalcogenide ligands to adopt various binding modes in molecular and polymeric complexes and the ability of the flux method to supply such ligands and to produce many novel structures has been exploited to form new solid-state polychalcogenides. Thus far, transition metals have received the most attention by this technique with main group metals not significantly investigated. The existence of several A/Ti/Q (A = alkali metal) compounds and the chemical Ti^{4+}/Sn^{4+} similarity prompted us to choose Sn as a main group metal for synthetic investigation in order to further probe this similarity. Out of several metal tin (poly)sulfides known, such as $(Et_4N)_2[Sn(S_4)_3]_{0.4}[Sn(S_4)_2(S_6)]_{0.6}$,[9] $Na_4SnS_4\cdot 14H_2O$,[10] $Na_4Sn_2S_6\cdot 14H_2O$,[11] and $Na_6Sn_2S_7$,[12] which contain discrete *molecular* anions, and the *polymeric* $K_2SnS_3\cdot 2H_2O$,[13] $Na_4Sn_3S_8$,[14] Na_2SnS_3,[15] and $Cs_4Sn_5S_{12}$,[16] only $(Et_4N)_2[Sn(S_4)_3]_{0.4}[Sn(S_4)_2(S_6)]_{0.6}$ contains polysulfide ligands. Among these, $Na_6Sn_2S_7$ and $Na_4Sn_3S_8$ were made by heating stoichiometric mixtures of Sn/Na_2S/S and SnS_2/Na_2S at 450 and 680 °C, respectively. $Cs_4Sn_5S_{12}$ was made hydrothermally with SnS_2 and Cs_2CO_3 at 130 °C. $(Et_4N)_2[Sn(S_4)_3]_{0.4}[Sn(S_4)_2(S_6)]_{0.6}$ was synthesized from $SnCl_2\cdot 2H_2O$ and ammonium polysulfide in acetone/methanol solution at 50 °C. The rest were synthesized using SnS_2 or $SnCl_4$ in reactions with monosulfides in aqueous solutions at ambient

(1) Sunshine, S. A.; Kang, D.; Ibers, J. A. *J. Chem. Soc.* **1987**, *109*, 6202–6204.
(2) Sunshine, S. A.; Kang, D.; Ibers, J. A. *Mater. Res. Soc. Symp. Proc.* **1987**, *97*, 391–396.
(3) Kanatzidis, M. G. *Chem. Mater.* **1990**, *2*, 353–363.
(4) Kanatzidis, M. G.; Park, Y. *J. Am. Chem. Soc.* **1989**, *111*, 3767–3769.
(5) Park, Y.; Kanatzidis, M. G. Manuscript in preparation.
(6) Kanatzidis, M. G.; Park, Y. *Angew Chem., Int. Ed. Engl.* **1990**, *29*, 914–915.
(7) Kanatzidis, M. G.; Park, Y. *Chem. Mater.* **1990**, *2*, 99–101.
(8) Park, Y.; DeGroot, D. C.; Schindler, J.; Kannewurf, C. R.; Kanatzidis, M. G. *Angew. Chem., Int. Ed. Engl.* **1991**, *30*, 1325–1328.
(9) Müller, A.; Schimanski, J.; Römer, M.; Bögge, H.; Baumann, F.-W.; Eltzner, W.; Krickemeyer, E.; Billerbeck, U. *Chimia* **1985**, *39*, 25–27.
(10) Schiwy, W.; Pohl, S.; Krebs, B. *Z. Anorg. Allg. Chem.* **1973**, *402*, 77–86.
(11) Krebs, B.; Pohl, S.; Schiwy, W. *Z. Anorg. Allg. Chem.* **1972**, *393*, 241–252.
(12) Krebs, B.; Schiwy, W. *Z. Anorg. Allg. Chem.* **1973**, *393*, 63–71.
(13) Schiwy, W.; Blutau, Chr.; Gäthje, D.; Krebs, B. *Z. Anorg. Allg. Chem.* **1975**, *412*, 1–10.
(14) Jumas, J.-C.; Philippot, E.; Maurin, M. *J. Solid State Chem.* **1975**, *14*, 152–159.
(15) Mark, W.; Lindqvist, O.; Jumas, J.-C.; Philippot, E. *Acta Crystallogr.* **1974**, *B30*, 2620–2628.
(16) Sheldrick, W. S. *Z. Anorg. Allg. Chem.* **1988**, *562*, 23–30.

0020-1669/93/1332-2453$04.00/0

temperature. Here we report the first five alkali metal tin polysulfides, $K_2Sn_2S_8$ (I), α-$Rb_2Sn_2S_8$ (II), β-$Rb_2Sn_2S_8$ (III), $Cs_2Sn_2S_6$ (V), and Cs_2SnS_{14} (VI), and one potassium tin sulfide, $K_2Sn_2S_5$ (IV), synthesized using alkali metal polychalcogenides as reactive fluxes.

Experimental Section

Synthesis. All work was done under a nitrogen atmosphere. Reagents: Sn metal was purchased from CERAC Inc., ~325 mesh, 99.8%. Sublimed sulfur was purchased from J. T. Baker Chemical Co., 99.5–100.5%. K_2S, Rb_2S, and Cs_2S starting materials were prepared by a modified literature procedure.[17] All the reagents are stored under N_2 in a glovebox.

Potassium Sulfide, K_2S. A 5.815-g amount (0.181 mol) of elemental sulfur was combined with 14.192 g (0.363 mol) of sliced potassium metal under nitrogen in a 250-mL round-bottom flask equipped with a Teflon valve and a stirring bar. An approximately 80-mL volume of liquid ammonia was condensed into the flask, which was kept at −78 °C by dry ice/acetone bath. The mixture was stirred for a couple of hours until the potassium metal was dissolved completely. When a dark blue solution formed, the ammonia was removed slowly by evaporation as the cold bath was allowed to warm up to room temperature under a flow of nitrogen. The resulting air-sensitive white solid was dried in vacuum overnight, flame-dried, ground to a fine powder, and kept in a N_2 glovebox.

Cesium Sulfide, Cs_2S. A 4.644-g amount (0.035 mol) of cesium metal was placed in a 250-mL round-bottom flask equipped with a Teflon valve in a N_2 glovebox. *Because cesium metal will react with Teflon and sulfur vigorously upon contact in the solid state (caution!)*, a 40-mL volume of liquid ammonia was first condensed into the flask kept at −78 °C by dry ice/acetone bath to dissolve the cesium metal. A sample of 0.561 g (0.0175 mol) of elemental sulfur and a Teflon stirring bar were then added to the dark blue solution. Approximately an additional 40 mL of liquid ammonia was condensed into the flask. The mixture was stirred for about 1 h. The subsequent procedure is the same as that for K_2S above. The resulting air-sensitive white fine powder was kept in a N_2 glovebox.

Rubidium Sulfide, Rb_2S. The procedure to prepare Rb_2S is the same as that of Cs_2S.

$K_2Sn_2S_8$ (I). A mixture of Sn metal (0.119 g, 1 mmol), K_2S (0.220 g, 2 mmol), and S (0.256 g, 8 mmol) in 1:2:8 ratio was loaded into a ~5-mL Pyrex tube in a N_2 glovebox. The tube was evacuated and flame sealed at the pressure of $\sim 10^{-3}$ Torr. The mixture was heated at 250 or 275 °C for 4–6 days. Upon cooling of the mixture to room temperature at the rate of 2 °C/h, small orange chunky crystals were formed. The crystals obtained at 275 °C are larger in size. The product was washed with water to remove excess K_2S_x flux and then washed with carbon disulfide to remove unreacted sulfur. The product is obtained in 86% yield (based on Sn metal). The homogeneity of the product was confirmed by comparison of the calculated and experimental X-ray powder diffraction patterns (see supplementary material). Semiquantitative elemental analyses were run on a scanning electron microscope (SEM) using an energy dispersive (EDS) microscope technique. EDS indicated the presence of three elements, K, Sn, and S, with a rough ratio of 2:2:7.9, which is very close to the chemical formula determined by single-crystal X-ray diffraction analysis.

α-$Rb_2Sn_2S_8$ (II). The preparation and isolation of II are similar to that of I. However, the mixture of Sn metal (0.119 g, 1 mmol), Rb_2S (0.406 g, 2 mmol), and S (0.256 g, 8 mmol) in 1:2:8 ratio at 270 °C for 4 days gave only ~38% yield, accompanied with white crystals of $Rb_4Sn_2S_6$ as an impurity.[18] Pure II was made and the yield was improved to 89%, when the reaction temperature was increased to 330 °C and the $Sn/Rb_2S/S$ ratio was 1:2:12. Upon cooling of the mixture at 2 °C/h, larger, well-formed orange needlelike crystals were obtained. The homogeneity of the product at 330 °C was confirmed by the comparison of experimental and calculated X-ray powder diffraction pattern (see supplementary material). SEM/EDS indicated the stoichiometry $Rb_{1.4}Sn_2S_9$. The Rb content is underestimated due to an artifact of the standardless program used. We found that a correction factor of ~1.5 must be applied.

β-$Rb_2Sn_2S_8$ (III). The preparation and isolation of III are also similar to those given above. The mixture of $Sn/Rb_2S/S$ in 1:1:8 ratio was heated to 450 °C for 4 days. Upon cooling of the mixture at 3 °C/h, orange thin platelike crystals of β-$Rb_2Sn_2S_8$ were obtained in the yield of ~59%. The homogeneity of the product was confirmed by comparison of the experimental and calculated X-ray diffraction powder pattern (see supplementary material). SEM/EDS indicated $Rb_{1.4}Sn_2S_9$.

$K_2Sn_2S_5$ (IV). The preparation and isolation of IV is the same as for I except that the reaction temperature was increased to 320 °C. However, a cooling rate of 2 °C/h, gave only yellow microcrystals at ~81% yield. In order to grow larger crystals for single-crystal X-ray analysis, we increased the reaction temperature to 400 °C. At this temperature, the yield of IV was very low (less than 10%) and the major product consisted of water-soluble white crystals of $K_4Sn_2S_6$.[18] The homogeneity of the air-stable, water-insoluble yellow product was confirmed by comparison of the calculated and experimental X-ray powder diffraction pattern. SEM/EDS indicated the presence of K, Sn, and S in a ratio of about 2:2:5.7.

$Cs_2Sn_2S_6$ (V). Pure yellow thin platelike crystals of V can be obtained under the same reaction conditions used for VI but using less sulfur ($Sn:Cs_2S:S$ = 1:3:8). However, crystals obtained at 275 °C had poor crystallinity. Crystals suitable for single-crystal X-ray diffraction analysis were obtained by heating a mixture of Sn (0.059 g, 0.5 mmol), Cs_2S (0.149 g, 0.5 mmol), and S (0.128 g, 4 mmol) in an evacuated Pyrex tube in 1:1:8 ratio at 400 °C for 4 days using a cooling rate of 4 °C/h. The product was isolated by washing with DMF to remove excess Cs_2S_x flux followed by washing with ether. The product is insoluble in water and common organic solvents. The yield was ~86% (based on Sn). Its homogeneity was confirmed by the comparison of the calculated and experimental X-ray powder diffraction patterns. SEM/EDS gave the approximate stoichiometry $Cs_2Sn_2S_{7.4}$.

Cs_2SnS_{14} (VI). The procedure for the preparation of VI is the same as that of I. Samples of Sn (0.059 g, 0.5 mmol) and Cs_2S (0.298 g, 1.0 mmol) were mixed with S in the range 0.096–0.160 g (3.0–5.0 mmol). The product was washed by methanol under N_2 to remove excess Cs_2S_x flux. All the three sulfur ratios gave a mixture of red crystals of VI and yellow crystalline V. The red crystals of VI dissolve slowly in water but are stable in air. Suitable crystals for X-ray diffraction studies were picked manually. SEM/EDS indicated the presence of Cs, Sn, and S in the ratio of about 2:1:15.

Physical Measurements. X-ray Diffraction. The X-ray powder diffraction patterns were recorded with a calibrated Phillips XRD-3000 controlled by a PDP 11 computer and operating at 40 kV/20 mA. Ni-filtered Cu radiation was used.

Electron Microscopy. Quantitative microprobe analysis was performed on a JEOL 35CF scanning electron microscope (SEM) equipped with Tracor Northern TN5500 X-ray microanalysis. The standardless quantitative (SQ) analysis program uses multiple least-squares analysis and a ZAF matrix correction procedure to calculate elemental concentration. Known compounds containing the elements of interest were used for calibration.

Infrared and Raman Spectroscopy. IR spectra were recorded as CsI pressed pellets with a computer-controlled Nicolet 740 Fourier transform infrared spectrometer in 4-cm^{-1} resolution. Raman spectra were obtained in backscattering geometry from solid samples in spinning EPR tubes at room temperature. The Raman equipment included a SPEX 1459 illuminator, a SPEX 1877 triplemate with an EG&G Model 1421 diode-array detector, and an OMA III computer. An Innova 200 argon-ion laser system was used to provide an excitation wavelength of 514.5 nm, and the power incident on the sample was 50 mW. The Raman spectral resolution was approximately 8 cm^{-1}.

UV/Vis/Near-IR Spectroscopy. Optical diffuse reflectance measurements were made at room temperature with a Shimadzu UV-3101PC double-beam, double-monochromator spectrophotometer. The instrument was equipped with an integrating sphere and controlled by a personal computer. The measurement of diffuse reflectivity can be used to obtain values for the band gap, which agree rather well with values obtained by absorption measurements from single crystals of the same material. The digitized spectra were processed using the Kaleidagraph software program. $BaSO_4$ powder was used as reference (100% reflectance). Absorption data were calculated from the reflectance data using the Kubelka–Munk[19] function: $\alpha/S = (1-R)^2/2R$. R is the reflectance at a given wavelength,

(17) Klemm, W.; Sodomann, H.; Langmesser, P. *Z. Anorg. Allg. Chem.* **1939**, *241*, 281–304.

(18) SEM/EDS semiquantitative elemental analyses on the white crystals obtained from the system $Sn/A_2S/S$ showed A, Sn, and S approximately in the stoichiometry $A_4Sn_2S_6$[11] (A = K, Rb, Cs): Liao, J.-H.; Kanatzidis, M. G. Unpublished work.

(19) (a) Wendlandt, W. W.; Hecht, H. G. *Reflectance Spectroscopy*; Interscience Publishers: New York, 1966. (b) Kotüm, G. *Reflectance Spectroscopy*; Springer Verlag: New York, 1969. (c) Tandon, S. P.; Gupta, J. P. *Phys. Stat. Solidi* **1970**, *38*, 363–367.

Table I. Data for Crystal Structure Analyses of $K_2Sn_2S_8$ (I), α-$Rb_2Sn_2S_8$ (II), β-$Rb_2Sn_2S_8$ (III), $K_2Sn_2S_5$ (IV), $Cs_2Sn_2S_6$ (V), and Cs_2SnS_{14} (VI)

formula	$K_2Sn_2S_8$ (I)	α-$Rb_2Sn_2S_8$ (II)	β-$Rb_2Sn_2S_8$ (III)	$K_2Sn_2S_5$ (IV)	$Cs_2Sn_2S_6$ (V)	Cs_2SnS_{14} (VI)
fw	572.06	664.80	664.80	475.88	695.56	833.34
a, Å	9.580(8)	9.788(3)	9.987(5)	11.804(3)	7.289(4)	6.964(6)
b, Å	10.004(5)	9.978(3)	19.635(3)	7.808(1)	7.597(3)	18.66(1)
c, Å	14.131(7)	14.360(2)	13.747(3)	11.539(1)	6.796(3)	14.80(1)
α, deg	90.0	90.0	90.0	90.0	114.80(3)	90.0
β, deg	107.82(6)	106.70(2)	90.0	108.35(1)	108.56(4)	99.39(1)
γ, deg	90.0	90.0	90.0	90.0	97.54(4)	90.0
Z; V, Å^3	4; 1289(3)	4; 1343(1)	8; 2696(2)	4; 947.8(5)	1; 308.1(7)	4; 1897(5)
space group	$P2_1/n$	$P2_1/n$	$Pbcn$	$C2/c$	$P\bar{1}$	$P2_1/n$
d_{calc}, g/cm^3	2.95	3.29	3.28	3.33	3.78	2.92
cryst size, mm	0.2 × 0.1 × 0.1	0.2 × 0.2 × 0.4	0.07 × 0.09 × 0.42	0.4 × 0.5 × 0.85	0.8 × 0.9 × 1.0	0.12 × 0.9 × 0.4
radiation	Mo Kα	Mo Kα	Mo Kα	Mo Kα	Mo Kα	Mo Kα
λ, Å	0.716 09	0.716 09	0.716 09	0.716 09	0.716 09	0.716 09
μ(Mo Kα), cm^{-1}	57.4	118.9	118.5	71.5	107.8	65.7
final R/R_w,[b] %	4.9/5.1	3.0/3.6	3.2/3.5	4.7/6.0	3.1/3.9	4.46/4.95

[a] At 23 °C. [b] $R = \sum||F_o| - |F_c||/\sum|F_o|$. $R_w = \{\sum w(|F_o| - |F_c|)^2/\sum w|F_o|^2\}^{1/2}$.

Table II. Positional Parameters and Equivalent Isotropic Displacement Values (Å^2)[a] for $K_2Sn_2Sn_8$ (I)

atom	x	y	z	B(eq)
Sn(1)	0.0325(1)	0.1710(1)	0.0178(1)	1.40(5)
Sn(2)	0.5940(1)	0.0001(1)	0.4050(1)	1.15(4)
K(1)	0.3506(5)	0.3631(5)	0.2038(4)	3.0(2)
K(2)	0.0310(6)	0.2733(6)	0.4072(4)	3.8(2)
S(1)	0.2196(5)	0.2742(5)	–0.0369(4)	1.6(2)
S(2)	–0.1670(5)	0.0428(5)	–0.0856(4)	1.9(2)
S(3)	0.6433(5)	–0.0983(5)	0.5783(3)	1.5(2)
S(4)	0.5089(5)	0.0668(5)	0.2194(3)	1.6(2)
S(5)	0.0121(5)	0.2708(5)	0.1662(3)	1.5(2)
S(6)	0.6924(6)	0.1425(5)	0.1947(4)	2.3(2)
S(7)	0.6912(5)	0.3438(5)	0.2300(4)	1.8(2)
S(8)	0.6440(5)	0.4413(5)	0.0965(3)	1.7(2)

[a] $B(eq) = (8\pi^2/3)\sum_{i=1}^{3}\sum_{j=1}^{2}U_{ij}a^*_i a^*_j \vec{a}_i \cdot \vec{a}_j$. Estimated standard deviations are given in parentheses.

Table III. Positional Parameters and Equivalent Isotropic Displacement Values (Å^2)[a] for α-$Rb_2Sn_2S_8$ (II)

atom	x	y	z	B(eq)
Sn(1)	0.02687(7)	0.17298(6)	0.01519(4)	1.42(2)
Sn(2)	0.59313(6)	–0.00021(6)	0.40486(4)	1.23(2)
Rb(1)	0.3511(1)	0.3664(1)	0.20466(8)	2.96(4)
Rb(2)	0.0292(1)	0.2751(1)	0.40894(8)	3.21(5)
S(1)	0.2105(2)	0.2743(2)	–0.0405(2)	1.62(9)
S(2)	–0.1655(2)	0.0379(2)	–0.0802(2)	1.89(9)
S(3)	0.6379(2)	–0.0999(2)	0.5747(2)	1.40(8)
S(4)	0.5109(2)	0.0666(2)	0.2236(2)	1.71(8)
S(5)	0.0078(2)	0.2702(2)	0.1628(2)	1.63(9)
S(6)	0.6894(3)	0.1408(2)	0.1948(2)	2.1(1)
S(7)	0.6944(2)	0.3426(2)	0.2290(2)	1.70(8)
S(8)	0.6514(2)	0.4418(2)	0.0987(2)	1.65(8)

[a] $B(eq) = (8\pi^2/3)\sum_{i=1}^{3}\sum_{j=1}^{3}U_{ij}a^*_i a^*_j \vec{a}_i \cdot \vec{a}_j$. Estimated standard deviations are given in parentheses.

α is the absorption coefficient, and S is the scattering coefficient. The scattering coefficient has been shown to be practically wavelength independent for particles larger than 5 μm, which is smaller than the particle size of the samples used here.

Single-Crystal X-Ray Diffraction Analyses. Because the orange crystals of $K_2Sn_2S_8$ (I) were small, the X-ray diffraction data were collected by Molecular Structure Corp. (MSC), The Woodlands, TX, using a rotating anode X-ray generator in order to obtain a sufficient number of reflections with reasonable intensity. An orange prismatic crystal was mounted on a glass fiber. All measurements were made on a Rigaku AFC6R diffractometer with graphite-monochromated Mo Kα radiation with a 12-kW rotating anode generator. Intensity data for I were measured at 23 °C using the ω–2θ scan mode. The stability of the experimental setup and crystal intensity were monitored by measuring three standard reflections periodically every 150 reflections. A decline of ~4.5% was observed, and a linear correction factor was applied to the data. An empirical absorption correction (based on ψ scans) was applied. The equivalent reflections were averaged. The structure of I was solved at MSC by direct methods (MITHRIL[20] and DIRDIF[21]) and refined by full-matrix least-square techniques.

The X-ray diffraction data of Cs_2SnS_{14} (VI) were collected on a P3 Nicolet four-circle diffractometer using the $\theta/2\theta$ scan mode and graphite-monochromated Mo Kα radiation. A red crystal of VI was mounted on the end of a glass fiber. The data were collected at 23 °C, and three check reflections were monitored every 100 reflections without evidence of any significant decay during the data collection period. An empirical absorption correction was applied to all the data (based on ψ scans). An additional absorption correction following the DIFABS[22] procedure was applied to isotropically refined data. The equivalent reflections were averaged. The structure refinement was done with the SDP[23] package of crystallographic program running on a VAXstation 2000 computer. The structure of VI was solved with direct methods (SHELXS-86),[24] and it was refined by full-matrix least-squares techniques.

The X-ray diffraction data of α-$Rb_2Sn_2S_8$ (II), β-$Rb_2Sn_2S_8$(III), $K_2Sn_2S_5$ (IV), and $Cs_2Sn_2S_6$ (V) were collected on a Rigaku AFC6S diffractometer using the ω-2θ scan mode and graphite-monochromated Mo Kα radiation at 23 °C. Those crystals were mounted on the end of glass fibers. The stability of the experimental setup and crystal intensity were monitored by measuring three standard reflections periodically for every 150 reflections. No significant decay was observed during the data collection. An empirical absorption correction was applied to the data (based on ψ scans). An additional absorption correction following the DIFABS procedure was applied to isotropically refined data. The equivalent reflections were averaged. The structure refinement was done wiht the TEXSAN[25] package of crystallographic programs running on a VAXstation 3100/76 computer. The structures of II–V were solved with direct methods (SHELXS-86), and they were refined by full-matrix least-squares techniques available in TEXSAN.

The crystallographic data and detailed information of structure solution and refinement for I–VI are listed in Table I. Atomic coordinates and equivalent isotropic thermal parameters and estimated standard deviations for I–VI are given in Tables II–VII, respectively.

Results and Discussion

Synthesis. All compounds were synthesized in A_2S_x fluxes (A = alkali metal). The molten alkali metal polysulfides formed by the *in situ* reaction of alkali metal sulfide and elemental sulfur serve as reaction media which enhance the mobilities of the reacting species and help the crystallization of the final products.

(20) MITHRIL: an Integrated Direct Methods Computer Program. Gilmore, C. J. *J. Appl. Crystallogr.* **1984**, *17*, 42–46.
(21) DIRDIF: Beurskens, P. T. DIRDIF: Direct Method for Difference Structures. An Automatic Procedure for Phase Extension and Refinement of Difference Structure Factors. Technical Report 1984/1 Crystallography Laboratory, Toernooiveld, 6525 Ed, Nijmegen, The Netherlands.
(22) DIFABS: Walker, N.; Stuart, D. DIFABS: An Emperical Method for Correcting Diffraction Data for Absorption Effects. *Acta Crystallogr.* **1983**, *A39*, 158–166.
(23) Fenz, B. A. The Enraf-Nonius CAD4 SDP System. In *Computing in Crystallography*; Delft University Press: Delft, Holland, 1978; pp 64–71.
(24) Sheldrick, G. M. In *Crystallographic Computing 3*; Sheldrick, G. M., Kruger, C., Goddard, R., Eds.; Oxford University Press: Oxford, U.K., 1985; pp 175–189.
(25) TEXSAN-TEXRAY Structure Analysis Package, Molecular Structure Corp., The Woodlands, TX, 1985.

Table IV. Positional Parameters and Equivalent Isotropic Displacement Values (Å²)[a] for β-$Rb_2Sn_2S_8$ (III)

atom	x	y	z	B(eq)
Sn(1)	0.17289(7)	0.32611(4)	0.27038(6)	1.38(3)
Sn(2)	0.5	0.41693(6)	0.25	1.17(5)
Sn(3)	0.5	0.22879(6)	0.25	1.23(5)
Rb(1)	0.2273(1)	0.42997(8)	−0.0359(1)	3.11(7)
Rb(2)	0.1393(1)	0.18813(8)	0.0284(1)	3.01(7)
S(1)	0.2778(3)	0.4240(2)	0.3385(2)	1.6(1)
S(2)	0.0379(3)	0.3318(2)	0.1264(2)	1.9(1)
S(3)	0.4008(3)	0.3232(2)	0.1427(2)	1.3(1)
S(4)	0.5637(3)	0.5084(2)	0.3775(2)	1.5(1)
S(5)	0.2661(3)	0.2219(2)	0.3307(2)	1.5(1)
S(6)	0.6557(3)	0.5796(2)	0.2909(2)	1.7(1)
S(7)	0.8589(3)	0.5604(2)	0.3018(3)	2.0(2)
S(8)	0.4377(3)	0.1399(2)	0.1207(2)	1.8(1)

[a] $B(\text{eq}) = (8\pi^2/3)\sum_{i=1}^{3}\sum_{j=1}^{3} U_{ij}a^*_i a^*_j \vec{a}_i \cdot \vec{a}_j$. Estimated standard deviations are given in parentheses.

Table V. Positional Parameters and Equivalent Isotropic Displacement Values (Å²)[a] for $K_2Sn_2S_5$ (IV)

atom	x	y	z	B(eq)
Sn	0.09424(8)	0.1539(1)	0.44164(7)	0.72(4)
K	−0.2801(3)	0.1680(4)	0.3173(3)	2.1(1)
S(1)	0.0170(3)	0.1340(5)	0.6163(3)	1.5(1)
S(2)	0	0.3141(6)	0.25	1.2(2)
S(3)	0.3039(3)	0.0516(4)	0.4619(3)	1.0(1)

[a] $B(\text{eq}) = (8\pi^2/3)\sum_{i=1}^{3}\sum_{j=1}^{3} U_{ij}a^*_i a^*_j \vec{a}_i \cdot \vec{a}_j$. Estimated standard deviations are given in parentheses.

Table VI. Positional Parameters and Equivalent Isotropic Displacement Values (Å²)[a] for $Cs_2Sn_2S_6$ (V)

atoms	x	y	z	B(eq)
Cs	0.1845(1)	0.8627(1)	0.2325(1)	1.87(2)
Sn	0.5135(1)	0.4257(1)	0.2224(1)	0.67(2)
S(1)	0.6075(4)	0.1129(4)	0.1701(5)	1.28(7)
S(2)	0.2345(4)	0.4348(4)	0.3383(5)	1.19(7)
S(3)	0.6997(4)	0.7104(4)	0.2193(5)	1.35(7)

[a] $B(\text{eq}) = (8\pi^2/3)\sum_{i=1}^{3}\sum_{j=1}^{3} U_{ij}a^*_i a^*_j \vec{a}_i \cdot \vec{a}_j$. Estimated standard deviations are given in parentheses.

Table VII. Positional Parameters and Equivalent Isotropic Displacement Values (Å²)[a] for Cs_2SnS_{14} (VI)

atom	x	y	z	B(eq)
Cs(1)	−0.0858(2)	0.80160(6)	0.47666(8)	4.37(6)
Cs(2)	0.6252(2)	0.95164(6)	−0.16319(8)	4.38(6)
Sn	0.0355(2)	0.82444(6)	0.16925(7)	2.77(5)
S(1)	0.2595(7)	0.8165(2)	0.3247(3)	3.7(2)
S(2)	0.4119(8)	0.9090(3)	0.3562(3)	4.9(3)
S(3)	0.267(1)	0.9672(3)	0.4438(3)	5.6(3)
S(4)	0.0815(9)	1.0348(3)	0.3631(3)	4.7(3)
S(5)	−0.1502(8)	0.9730(2)	0.3083(3)	4.0(2)
S(6)	−0.1128(8)	0.9504(2)	0.1770(3)	3.9(2)
S(7)	0.3328(7)	0.8643(2)	0.0983(3)	3.4(2)
S(8)	0.2004(7)	0.9114(3)	−0.0226(3)	3.8(2)
S(9)	0.0152(8)	0.8311(3)	−0.0794(3)	4.0(2)
S(10)	−0.1810(7)	0.8260(3)	0.0104(3)	3.8(2)
S(11)	0.1443(8)	0.6934(2)	0.1627(3)	4.3(2)
S(12)	−0.1178(9)	0.6430(3)	0.1328(3)	4.6(3)
S(13)	−0.2514(8)	0.6734(3)	0.2415(3)	4.6(2)
S(14)	−0.2782(7)	0.7823(2)	0.2266(3)	3.6(2)

[a] $B(\text{eq}) = (8\pi^2/3)\sum_{i=1}^{3}\sum_{j=1}^{3} U_{ij}a^*_i a^*_j \vec{a}_i \cdot \vec{a}_j$. Estimated standard deviations are given in parentheses.

In addition, the polysulfide melts are oxidizing agents which oxidize the Sn metal to the 4+ oxidation state as shown in eq 1. The chelating ability of S_x^{2-} units and the many modes by

$$Sn + S_x^{2-} \rightarrow Sn^{4+} + S_p^{2-} + S_q^{2-} + S_t^{2-} \qquad (1)$$

$$p + q + t = x$$

which they can link metal centers are responsible for the great diversity of new structures that can be accessed. When alkali

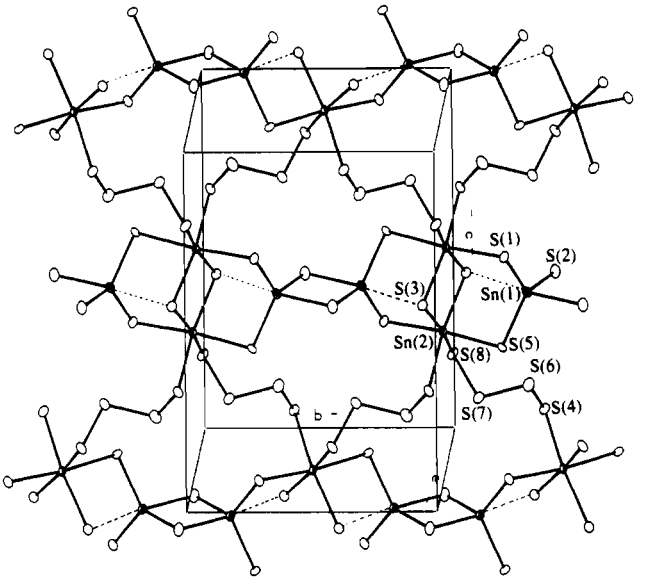

Figure 1. ORTEP representation and labeling scheme of the layered structure of $[Sn_2S_8]_n^{2n-}$ in I. The dashed lines indicate the shortest nonbonding Sn–S contacts (at 2.934(5) Å).

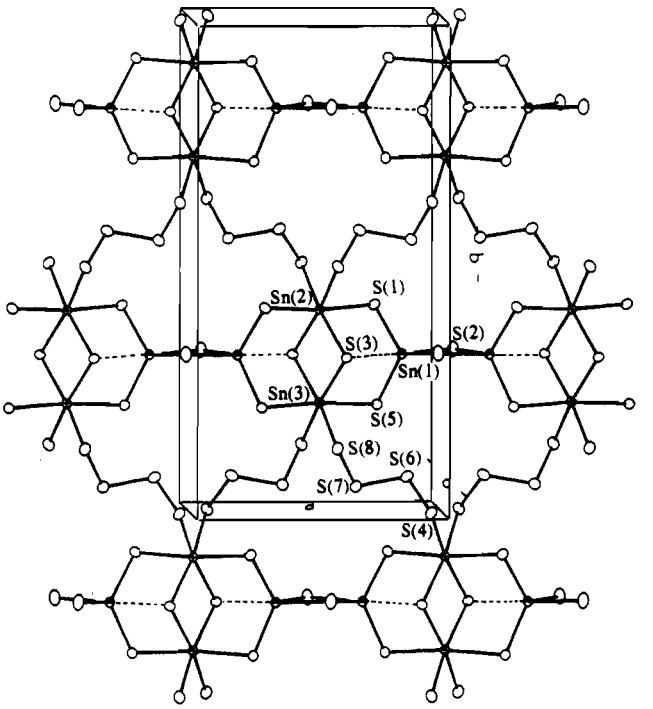

Figure 2. ORTEP representation and labeling scheme of the layered structure of $[Sn_2S_8]_n^{2n-}$ in III.

polysulfide salts melt, there are equilibria established between the various polysulfides, simplistically shown in eq 2. The direction

$$2A_2S_x \rightarrow A_2S_{x-y} + A_2S_{x+y} \qquad (2)$$

of equilibria can be controlled by temperature, the nature of the metal, and the value of x in S_x^{2-}. In general, higher temperatures promote the crystallization of larger and better crystals, but these temperatures are generally unfavorable for the stabilization of longer polysulfide chains, because they tend to break down to shorter chains and sulfur. In some cases, more elemental sulfur can be added to shift the equilibrium.

In the reaction of Sn with alkali metal polysulfides, we found that basic fluxes ($A_2S/S > 3/8$; A = K, Rb, Cs) favored formation of $A_4Sn_2S_6$,[18] which contains the molecular anion $[Sn_2S_6]^{4-}$. The structure of $[Sn_2S_6]^{4-}$ anions is an edge-sharing bitetrahedron. On examination of the extended structures of I–V, which were

Table VIII. Comparison of Bond Distances (Å) and Angles (deg) of $K_2Sn_2S_8$ (I), α-$Rb_2Sn_2S_8$ (II), and β-$Rb_2Sn_2S_8$ (III)

	$K_2Sn_2S_8$ (I)	α-$Rb_2Sn_2S_8$ (II)		β-$Rb_2Sn_2S_8$ (III)		$K_2Sn_2S_8$ (I)	α-$Rb_2Sn_2S_8$ (II)		β-$Rb_2Sn_2S_8$ (III)
				Tetrahedral Tin					
Sn(1)–S(1)	2.391(5)	2.392(2)	Sn(1)–S(1)	2.381(3)	Sn(1)···S(3)	2.934(5)	2.865(2)	Sn(1)···S(3)	2.875(3)
Sn(1)–S(2)	2.392(5)	2.399(2)	Sn(1)–S(2)	2.398(3)	Sn(1)–S(5)	2.386(5)	2.387(2)	Sn(1)–S(5)	2.397(3)
Sn(1)–S(2)	2.530(5)	2.532(2)	Sn(1)–S(2)	2.541(3)					
				Octahedral Tin					
Sn(2)–S(1)	2.574(5)	2.549(2)	Sn(2)–S(1)	2.535(3)	S(4)–S(6)	2.039(7)	2.047(3)	S(4)–S(6)	2.053(5)
Sn(2)–S(3)	2.547(5)	2.553(2)	Sn(2)–S(3)	2.559(3)	S(6)–S(7)	2.071(6)	2.069(3)	S(6)–S(7)	2.069(4)
Sn(2)–S(3)	2.551(5)	2.565(2)	Sn(3)–S(3)	2.567(3)	S(7)–S(8)	2.050(6)	2.050(3)	S(7)–S(8)	2.047(5)
Sn(2)–S(4)	2.584(5)	2.582(2)	Sn(2)–S(4)	2.589(3)	mean S-S	2.05(2)	2.06(1)		2.06(1)
Sn(2)–S(5)	2.585(5)	2.573(2)	Sn(3)–S(5)	2.589(3)	Sn(1)–Sn(1)	3.486(3)	3.500(2)	Sn(1)–Sn(1)	3.498(2)
Sn(2)–S(8)	2.585(5)	2.581(2)	Sn(3)–S(8)	2.568(3)	Sn(1)–Sn(2)	3.780(2)	3.756(1)	Sn(1)–S(2)	3.732(2)
mean Sn_{oct}-S	2.57(2)	2.57(1)	mean Sn_{oct}-S	2.57(2)	Sn(1)–Sn(2)	3.783(2)	3.766(1)	Sn(1)–Sn(3)	3.795(2)
					Sn(2)–Sn(2)	3.663(3)	3.695(1)	Sn(2)–Sn(3)	3.694(2)

	$K_2Sn_2S_8$ (I)[a]		α-$Rb_2Sn_2S_8$ (II)[a]		β-$Rb_2Sn_2S_8$ (III)[a]		$K_2Sn_2S_8$ (I)[a]		α-$Rb_2Sn_2S_8$ (II)[a]		β-$Rb_2Sn_2S_8$ (III)[a]
K(1)–S(1)	3.366(7)	Rb(1)–S(1)	3.515(3)	Rb(1)–S(1)	3.385(4)	K(2)–S(2)	3.404(7)	Rb(2)–S(2)	3.489(3)	Rb(1)–S(8)	3.406(4)
K(1)–S(2)	3.171(7)	Rb(1)–S(2)	3.282(3)	Rb(1)–S(2)	3.503(4)	K(2)–S(3)	3.530(7)	Rb(2)–S(3)	3.646(3)	Rb(2)–S(1)	3.531(4)
K(1)–S(3)	3.238(6)	Rb(1)–S(3)	3.321(3)	Rb(1)–S(3)	3.665(3)	K(2)–S(4)	3.400(7)	Rb(2)–S(4)	3.436(3)	Rb(2)–S(3)	3.286(4)
K(1)–S(4)	3.303(6)	Rb(1)–S(4)	3.351(3)	Rb(1)–S(4)	3.765(4)	K(2)–S(5)	3.353(7)	Rb(2)–S(5)	3.480(3)	Rb(2)–S(3)	3.355(3)
K(1)–S(5)	3.255(7)	Rb(1)–S(5)	3.378(3)	Rb(1)–S(4)	3.387(4)	K(2)–S(7)	3.515(7)	Rb(2)–S(7)	3.606(3)	Rb(2)–S(5)	3.376(4)
K(1)–S(7)	3.177(7)	Rb(1)–S(7)	3.286(3)	Rb(1)–S(5)	3.501(4)	K(2)–S(8)	3.343(7)	Rb(2)–S(8)	3.416(3)	Rb(2)–S(6)	3.278(4)
K(1)–S(8)	3.664(8)	Rb(1)–S(8)	3.754(3)	Rb(1)–S(6)	3.700(4)	K(2)–S(8)	3.714(8)	Rb(2)–S(8)	3.753(3)	Rb(2)–S(8)	3.374(4)
K(2)–S(1)	3.346(7)	Rb(2)–S(1)	3.435(3)	Rb(1)–S(7)	3.760(4)						

	$K_2Sn_2S_8$ (I)	α-$Rb_2Sn_2S_8$ (II)		β-$Rb_2Sn_2S_8$ (III)		$K_2Sn_2S_8$ (I)	α-$Rb_2Sn_2S_8$ (II)		β-$Rb_2Sn_2S_8$ (III)
S(1)–Sn(1)–S(2)	124.8(2)	126.04(9)	S(1)–Sn(1)–S(2)	122.3(1)	S(3)–Sn(2)–S(8)	91.5(2)	91.74(7)	S(3)–Sn(2)–S(4)	90.8(1)
S(1)–Sn(1)–S(2)	98.2(2)	95.76(8)	S(1)–Sn(1)–S(2)	96.3(1)	S(3)–Sn(2)–S(4)	88.9(2)	89.14(7)	S(3)–Sn(3)–S(8)	90.0(1)
S(1)–Sn(1)–S(5)	112.0(2)	112.55(8)	S(1)–Sn(1)–S(5)	112.5(1)	S(3)–Sn(2)–S(5)	97.0(2)	97.73(8)	S(3)–Sn(3)–S(5)	98.0(1)
S(2)–Sn(1)–S(2)	89.9(2)	89.60(8)	S(2)–Sn(1)–S(2)	89.6(1)	S(3)–Sn(2)–S(8)	169.4(1)	168.6(6)	S(3)–Sn(3)–S(8)	169.1(1)
S(2)–Sn(1)–S(5)	119.8(2)	119.12(9)	S(2)–Sn(1)–S(5)	122.9(1)	S(4)–Sn(2)–S(5)	82.5(1)	82.78(7)	S(5)–Sn(3)–S(8)	83.5(1)
S(2)–Sn(1)–S(5)	101.0(2)	100.40(8)	S(2)–Sn(1)–S(5)	99.6(1)	S(4)–Sn(2)–S(8)	93.2(2)	93.49(8)	S(4)–Sn(2)–S(4)	92.1(2)
S(1)–Sn(2)–S(3)	95.8(2)	96.43(8)	S(1)–Sn(2)–S(3)	95.8(1)				S(8)–Sn(3)–S(8)	94.3(2)
S(1)–Sn(2)–S(3)	88.5(2)	87.41(7)	S(1)–Sn(2)–S(3)	88.7(1)	S(5)–Sn(2)–S(8)	93.6(2)	93.54(8)	S(5)–Sn(3)–S(8)	92.4(1)
S(1)–Sn(2)–S(4)	93.9(1)	93.68(8)	S(1)–Sn(2)–S(4)	94.1(1)	Sn(1)–S(1)–Sn(2)	99.2(2)	99.28(8)	Sn(1)–S(1)–Sn(2)	98.7(1)
S(1)–Sn(2)–S(5)	173.3(2)	173.69(7)	S(1)–Sn(2)–S(1)	173.7(2)	Sn(1)–S(2)–Sn(1)	90.1(2)	90.40(8)	Sn(1)–S(2)–Sn(1)	90.2(1)
			S(5)–Sn(3)–S(5)	174.0(2)	Sn(2)–S(3)–Sn(2)	91.9(1)	92.43(7)	Sn(2)–S(3)–Sn(3)	92.22(9)
S(1)–Sn(2)–S(8)	80.9(1)	81.42(7)	S(1)–Sn(2)–S(4)	81.5(1)	Sn(2)–S(4)–S(6)	104.4(2)	105.1(1)	Sn(3)–S(8)–S(7)	104.5(2)
S(3)–Sn(2)–S(3)	88.1(1)	87.5(7)	S(3)–Sn(2)–S(3)	88.0(1)	Sn(1)–S(5)–Sn(2)	99.0(2)	98.38(8)	Sn(1)–S(5)–Sn(3)	99.1(1)
			S(3)–Sn(3)–S(3)	87.6(1)	S(4)–S(6)–S(7)	104.5(3)	105.5(1)	S(4)–S(6)–S(7)	105.8(2)
S(3)–Sn(2)–S(4)	169.8(1)	169.21(7)	S(3)–Sn(2)–S(4)	169.95(9)	S(6)–S(7)–S(8)	105.0(3)	105.6(1)	S(6)–S(7)–S(8)	106.0(2)
S(3)–Sn(2)–S(5)	88.1(1)	87.48(7)	S(3)–Sn(3)–S(5)	86.3(1)	Sn(2)–S(8)–S(7)	100.0(2)	100.4(1)	Sn(2)–S(4)–S(6)	100.9(2)

[a] Mean K–S = 3.39(16) Å (I) and mean Rb–S = 3.48(15) (II) and 3.48(17) Å (III).

formed with $A_2S/S < 3/8$, it appears that they are composed of fused $[Sn_2S_6]^{4-}$ units as building blocks linked by polysulfide chains (vide infra). Interestingly, the least basic flux in the Cs/Sn/S system afforded Cs_2SnS_{14}, containing exclusively polysulfide ligands in a discrete complex.

$Rb_2Sn_2S_8$ was found in two slightly different phases, the α-form made at lower temperature of 330 °C and the β-form formed at 450 °C in a sulfur-rich flux. The high temperature promotes the transition from the kinetically stable α-$Rb_2Sn_2S_8$ to the possibly thermodynamically more stable β-$Rb_2Sn_2S_8$. The β-form of $K_2Sn_2S_8$ has not been observed.

I–V are semiconductors and have very low room temperature conductivities ($<10^{-7}$ S/cm).

Structures of $K_2Sn_2S_8$, α-$Rb_2Sn_2S_8$, and β-$Rb_2Sn_2S_8$. These compounds have unique layered structures and are the first known tin–polysulfide framework solids. The anionic structures of I and II are identical, while that of III is a conformational isomer. They all contain two distinct Sn sites, one tetrahedral and one octahedral. These Sn centers are linked via S^{2-} and S_4^{2-} so the layered anionic framework can be expressed by the more descriptive formulation, $[Sn_2S_4(S_4)]^{2-}$. By assignment of the formal oxidation states of A^+ (A = K, Rb), S^{2-}, and S_4^{2-}, the formal oxidation state of Sn atoms at both sites in I–III is +4. After $ACuS_4$, these structures are the only other examples of compounds incorporating tetrasulfides in an extended solid-state framework. On the basis of the chemical similarity of Sn^{4+} and Ti^{4+}, the closest analogs of these compounds may be the Ti^{4+} compounds $K_4Ti_3S_{14}$ and $Na_2Ti_2Se_8$.[26] These compounds were also made from polychalcogenide melts in the temperature range 345–470 °C. Obviously, Sn does not undergo similar chemistry since I–III are not isostructural to $Na_2Ti_2Se_8$.

The two-dimensional structures of I and II are shown in Figure 1. I and II crystallize in the same monoclinic space group, the only significant difference being the larger interlayer spacing in II due to the larger size of Rb^+ compared to K^+. The higher temperature product, III, has its layers shifted slightly along the [102] crystallographic axis relative to II to form a more symmetric orthorhombic lattice as shown in Figure 2. The comparison of selected bond distances and angles of I–III are given in Table VIII. A stereoview of α-$Rb_2Sn_2S_8$ is shown in Figure 3.

The anionic layers of I–III are formed by a special arrangement of SnS_4 tetrahedra, SnS_6 octahedra, and S_4^{2-} ligands. The Sn^{4+} centers are divided into two sets of recognizable dimeric units, one of which involves the tetrahedral and the other the octahedral centers, as shown in Chart I. In the first kind, two distorted SnS_4 tetrahedra share an edge to form a Sn_2S_6 unit with a center of

(26) Kang, D.; Ibers, J. A. *Inorg. Chem.* **1988**, *27*, 549–551.

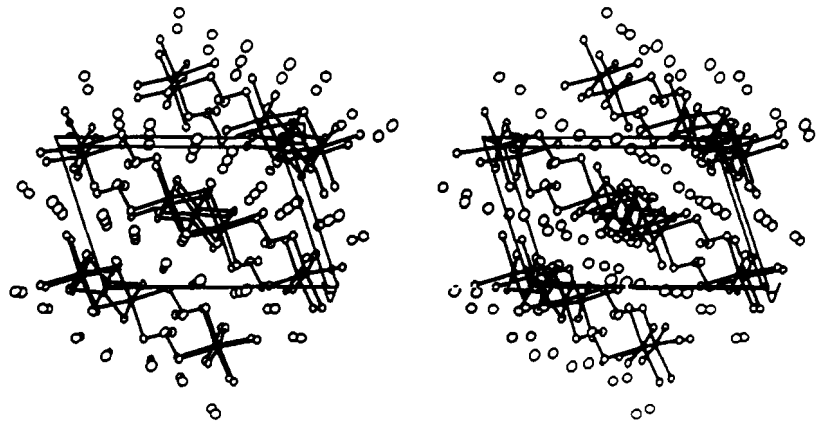

Figure 3. Stereoview of the unit cell of α-$Rb_2Sn_2S_8$.

Chart I

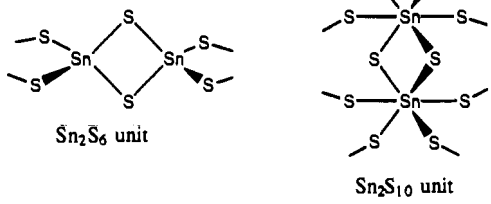

Chart II

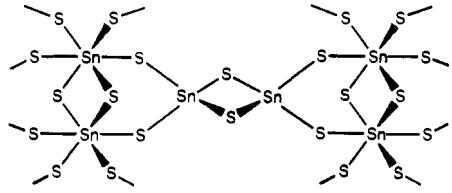

inversion in the middle of the shared edge. In the second, two slightly distorted SnS_6 octahedra share an edge through two equatorial S atoms to form a Sn_2S_{10} unit possessing a center of inversion at the middle of the edge. The Sn–Sn vectors in the Sn_2S_{10} units are oriented perpendicular to the corresponding Sn–Sn vectors in the Sn_2S_6 units. The two different dimeric units are linked together in an alternating fashion by sharing tetrahedral edges and octahedral corners, as shown in Chart II. This results in a set of parallel linear $[Sn_4S_{12}]_n$ chains running in the direction of the *b*-axis in I and II and the *a*-axis in III. The remaining four equatorial S atoms in the Sn_2S_{10} unit are actually the terminal atoms of S_4^{2-} ligands which link these $[Sn_4S_{12}]_n$ chains to form layers which are parallel to [101] crystallographic plane in I and II and parallel to [001] in III.

The Sn_2S_6 unit is found in isolated form in $Na_4Sn_2S_6 \cdot 14H_2O$.[11] However, in I–III the two averaged Sn(1)–S(2) distances are significantly different, 2.396(4) and 2.534(6) Å, while, in $Na_4Sn_2S_6 \cdot 14H_2O$, the corresponding Sn–S distances are more equal at 2.452 and 2.448 Å, respectively. A short contact between the distorted tetrahedral Sn atom and the bridging S(3) atom of the Sn_2S_2 core in the Sn_2S_{10} unit, as shown by the dashed lines in Figures 1 and 2, is responsible for the asymmetry of the Sn_2S_2 core in the Sn_2S_6 unit. This partial Sn···S bond formation, 2.934(5), 2.865(2), and 2.875(3) Å in I–III, respectively, causes a lengthening of Sn–S bond opposite to the Sn···S short contact. The average Sn(1)–S(1) and Sn(1)–S(5) distances are 2.388(6) and 2.390(6) Å, which are expectedly slightly longer than the terminal Sn–S distances in $Na_4Sn_2S_6 \cdot 14H_2O$, 2.325 and 2.338 Å. This is due to the bridging character of S(1) and S(5) linking Sn(1) and Sn(2). Bond angles in the Sn_2S_6 unit are similar to those in $Na_4Sn_2S_6 \cdot 14H_2O$. The S(2)–Sn(1)–S(2) angles are close to 90°. If the Sn···S(3) short contact is considered to be a bond, the coordination environment around Sn(1) can be viewed as a

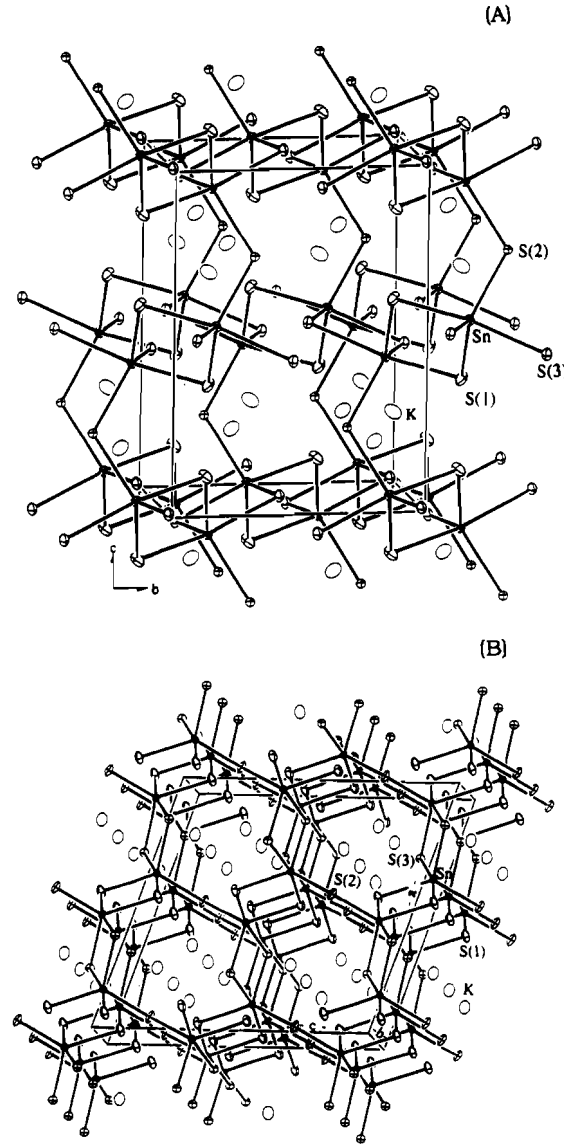

Figure 4. Structure and labeling scheme of $K_2Sn_2S_5$: (A) View down the *a*-axis; (B) view down the *b*-axis.

distorted trigonal bipyramid with an elongated axial Sn–S bond. One of the bridging sulfur atoms opposite to the Sn···S(3) short contact in the Sn_2S_2 core forms the other axial Sn–S bond in the trigonal bipyramid. The S(axial)–Sn(1)–S(axial) angles in I–III are 173.9(1), 174.9(1), and 176.1(1)°, respectively, while the average S(equatorial)–Sn(1)–S(equatorial) angles average 112.4(3), 121(2), and 124(2)°, respectively.

The average Sn–S distance, 2.57(2) Å, in the Sn_2S_{10} unit is very close to 2.571 Å found in $K_2SnS_3 \cdot 2H_2O$,[13] which is in the

Table IX. Comparison of Selected Bond Distances (Å) and Angles (deg) of $K_2Sn_2S_5$ (IV) and $Tl_2Sn_2S_5$

	$K_2Sn_2S_5$ (IV)	$Tl_2Sn_2S_5$		$K_2Sn_2S_5$ (IV)	$Tl_2Sn_2S_5$
Sn–S(1)[a]	2.430(3)	2.446(4)	K or Tl-S(1)	3.640(5)	3.711(4)
Sn–S(1)	2.550(4)	2.543(4)	K or Tl-S(2)	3.614(4)	3.615(2)
Sn–S(2)	2.468(2)	2.463(3)	K or Tl-S(2)	3.604(5)	3.586(4)
Sn–S(3)	2.398(3)	2.409(4)	K or Tl-S(3)	3.277(5)	3.269(4)
Sn–S(3)	2.648(3)	2.623(4)	K or Tl-S(3)	3.412(5)	3.339(4)
K or Tl-S(1)	3.090(5)	3.073(4)	K or Tl-S(3)	3.150(5)	3.160(4)
K or Tl-S(1)	3.337(5)	3.269(4)			

	$K_2Sn_2S_5$ (IV)	$Tl_2Sn_2S_5$		$K_2Sn_2S_5$ (IV)	$Tl_2Sn_2S_5$
S(1)–Sn–S(1)	83.9(1)	84.1(1)	S(2)–Sn–S(3)	112.33(8)	112.5(1)
S(1)–Sn–S(2)	128.0(1)	126.2(1)	S(2)–Sn–S(3)	86.6(1)	86.3(1)
S(1)–Sn–S(3)	118.8(1)	120.2(1)	S(3)–Sn–S(3)	88.6(1)	88.3(1)
S(1)–Sn–S(3)	85.5(1)	85.1(1)	Sn–S(1)–Sn	96.1(1)	95.9(1)
S(1)–Sn–S(2)	100.3(1)	102.0(1)	Sn–S(2)–Sn	119.1(2)	117.6(1)
S(1)–Sn–S(3)	96.1(1)	95.1(1)	Sn–S(3)–Sn	91.4(1)	91.7(1)
S(1)–Sn–S(3)	169.4(1)	169.0(1)			

[a] Mean Sn–S = 2.50(10) Å; mean K–S = 3.39(21) Å.

Chart III

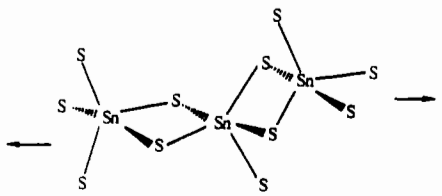

range of typical Sn–S distances in SnS_6 octahedra. The S–Sn–S angles are close to those of an ideal octahedron; see Table VIII.

The tetrasulfides linking the Sn_2S_{10} units possess helical conformation. The dihedral angles between the two outer S–S bonds are similar at 109.4(3), 110.4(1), and 109.8(2) for I–III, respectively. The averaged central S–S bond distance, 2.070(1) Å, is slightly longer than the averaged terminal S–S bond distance, 2.048(5) Å, while, in the free tetrasulfide anion in BaS_4,[27] no significant variation among the S–S distances is observed. The average S–S bond distance in BaS_4 is 2.069(2) Å.

The charge compensating cations are located between layers, as shown in Figure 3. There are two distinct K^+ or Rb^+ cations in I–III. In I and II, both K^+ and Rb^+ have similar coordination environments. There are two distinct K^+ or Rb^+ cations which are surrounded by seven and eight S atoms, respectively. The coordination environment of the two Rb^+ cations in III is nine and six S atoms, respectively. The average K–S distance for I is 3.39(16) Å, while the average Rb–S distances are 3.48(15) Å for II and 3.48(17) Å for III.

Structure of $K_2Sn_2S_5$. IV has a three-dimensional structure which is shown in Figure 4. Selected bond distances and angles are given in Table IX. This compound is isostructural to the Tl^+ salt, $Tl_2Sn_2S_5$,[28] which has been synthesized by heating a stoichiometric mixture of Tl, Sn, and S elements at 300 °C. The anionic structure of IV and $Tl_2Sn_2S_5$ and the relative positions of Tl^+ and K^+ to S atoms in the anion framework are approximately the same because of the similarity of the ionic radii of Tl^+ and K^+. The bond distances and angles are almost the same as in $Tl_2Sn_2S_5$. While this manuscript was in preparation, we learned that IV was synthesized by heating the stoichiometric mixture of $K_2S/Sn/S$ at 1070 K.[29] IV's selenium analogs $K_2Sn_2Se_5$[29] and $Rb_2Sn_2Se_5$[30] are also known and have been prepared by a high-temperature solid-state reaction and methanothermal reaction, respectively. This suggests that this structure type has considerable thermodynamic stability.

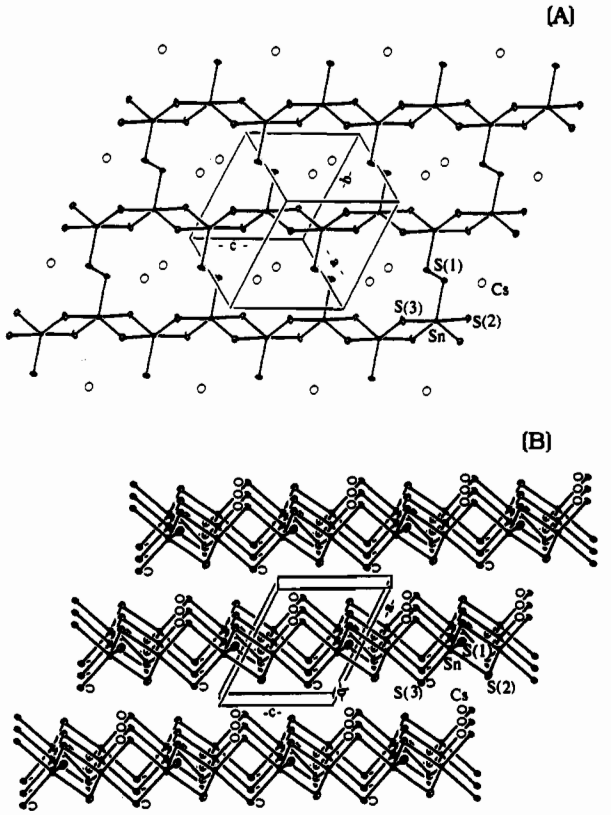

Figure 5. (A) ORTEP representation and labeling scheme of $Cs_2Sn_2S_6$ and (B) packing diagram of $Cs_2Sn_2S_6$ with a view down the *b*-axis.

Table X. Selected Distances (Å) and Angles (deg) for $Cs_2Sn_2S_6$ (V)

Sn–S(1)	2.473(3)	Cs–S(1)	3.767(3)
Sn–S(2)	2.402(3)	Cs–S(1)	3.643(3)
Sn–S(2)	2.599(3)	Cs–S(2)	3.650(3)
Sn–S(3)	2.410(3)	Cs–S(2)	3.575(4)
Sn–S(3)	2.550(3)	Cs–S(2)	4.041(3)
mean Sn–S	2.49(9)	Cs–S(3)	3.531(3)
S(1)–S(1)	2.099(6)	Cs–S(3)	3.501(3)
Cs–S(1)	3.580(3)	mean Cs–S	3.66(17)
S(1)–Sn–S(2)	110.5(1)	S(2)–Sn–S(3)	89.7(1)
S(1)–Sn–S(2)	82.4(1)	S(2)–Sn–S(3)	173.71(9)
S(1)–Sn–S(3)	126.1(1)	S(3)–Sn–S(3)	86.8(1)
S(1)–Sn–S(3)	95.5(1)	Sn–S(1)–S(1)	104.0(2)
S(2)–Sn–S(2)	90.1(1)	Sn–S(2)–Sn	89.9(1)
S(2)–Sn–S(3)	122.7(1)	Sn–S(3)–Sn	93.2(1)
S(2)–Sn–S(3)	96.2(1)		

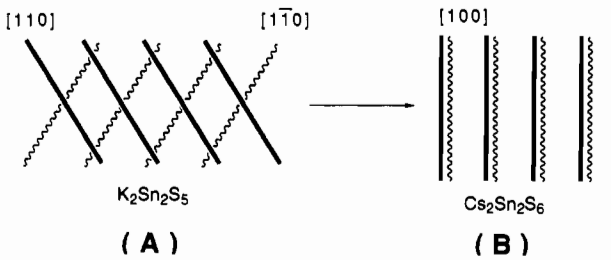

Figure 6. Schematic comparison of the orientations of the $(SnS_2)_n$ chains in $K_2Sn_2S_5$ and $Cs_2Sn_2S_6$. Black solid lines represent $(SnS_2)_n$ chains lying above, while wavy lines represent $(SnS_2)_n$ chains lying below the plane of the paper. (A) shows two parallel sets of $(SnS_2)_n$ chains in $K_2Sn_2S_5$ oriented along the [110] and [1$\bar{1}$0] directions, respectively, and linked by S^{2-}. (B) shows parallel sets of $(SnS_2)_n$ chains in $Cs_2Sn_2S_6$ oriented along the [100] direction and linked by S_2^{2-}.

Unlike I–III, which feature both four-coordinate and six-coordinate Sn atoms, IV features only five-coordinate Sn centers. The anionic framework in IV has SnS_5 distorted trigonal bipyramids as building blocks which share two of their common edges (formed by an axial S atom and an equatorial S atom) with one another to form $[SnS_3]_n^{2n-}$ chains (see Chart III) running in

(27) Abrahams, S. C.; Bernstein, J. L. *Acta Crystallogr.* **1969**, *25B*, 2365–2370.
(28) Eulenberger, G. *Z. Naturforsch.* **1981**, *366*, 687–690.
(29) Klepp, K. O. *Z. Naturforsch.* **1992**, *47b*, 197–200.
(30) Sheldrick, W. S.; Braunbeck, H.-G. *Z. Naturforsch.* **1992**, *476*, 151–153.

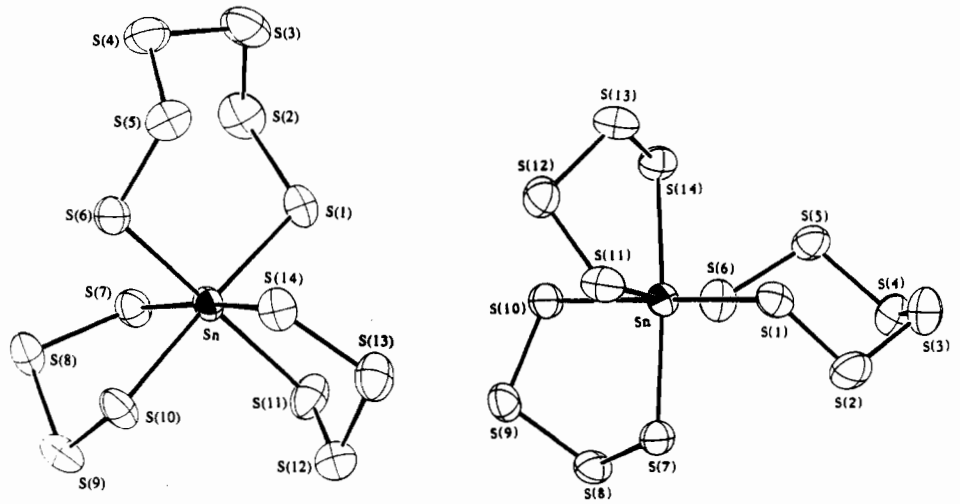

Figure 7. Two views and labeling scheme of the $[Sn(S_4)_2(S_6)]^{2-}$ anion.

Table XI. Selected Distances (Å) and Angles (deg) for Cs_2SnS_{14} (VI)

Sn–S(1)	2.555(4)	S(12)–S(13)	2.067(8)
Sn–S(6)	2.580(5)	S(13)–S(14)	2.056(7)
Sn–S(7)	2.576(5)	mean(S–S)	2.054(12)
Sn–S(10)	2.578(4)	Cs(1)–S(1)	3.560(5)
Sn–S(11)	2.567(5)	Cs(1)–S(7)	3.672(5)
Sn–S(14)	2.594(5)	Cs(1)–S(9)	3.715(6)
mean Sn–S	2.58(1)	Cs(1)–S(10)	3.664(5)
S(1)–S(2)	2.043(8)	Cs(1)–S(11)	3.577(6)
S(2)–S(3)	2.074(9)	Cs(1)–S(14)	3.739(5)
S(3)–S(4)	2.038(8)	Cs(2)–S(7)	3.568(5)
S(4)–S(5)	2.041(7)	Cs(2)–S(9)	3.587(5)
S(5)–S(6)	2.050(7)	Cs(2)–S(10)	3.574(5)
S(7)–S(8)	2.060(6)	Cs(2)–S(11)	3.752(5)
S(8)–S(9)	2.067(7)	Cs(2)–S(12)	3.665(5)
S(9)–S(10)	2.058(7)	Cs(2)–S(13)	3.618(5)
S(11)–S(12)	2.041(8)	mean(Cs–S)	3.64(7)
S(1)–Sn–S(6)	101.6(2)	Sn–S(1)–S(2)	112.2(2)
S(1)–Sn–S(7)	88.5(2)	Sn–S(6)–S(5)	110.1(2)
S(1)–Sn–S(10)	177.0(2)	Sn–S(7)–S(8)	101.7(2)
S(1)–Sn–S(11)	80.7(2)	Sn–S(10)–S(9)	103.9(2)
S(1)–Sn–S(14)	96.3(2)	Sn–S(11)–S(12)	100.7(3)
S(6)–Sn–S(7)	96.3(2)	Sn–S(14)–S(13)	105.5(3)
S(6)–Sn–S(10)	81.4(2)	S(1)–S(2)–S(3)	107.7(3)
S(6)–Sn–S(11)	173.5(2)	S(2)–S(3)–S(4)	106.5(3)
S(6)–Sn–S(14)	83.9(2)	S(3)–S(4)–S(5)	105.1(3)
S(7)–Sn–S(10)	90.7(2)	S(4)–S(5)–S(6)	106.0(3)
S(7)–Sn–S(11)	89.9(2)	S(7)–S(8)–S(9)	102.0(3)
S(7)–Sn–S(14)	175.1(1)	S(8)–S(9)–S(10)	101.7(3)
S(10)–Sn–S(11)	96.4(2)	S(11)–S(12)–S(13)	101.9(3)
S(10)–Sn–S(14)	84.5(2)	S(12)–S(13)–S(14)	103.5(3)
S(11)–Sn–S(14)	89.8(2)		

Table XII. IR and Raman Frequencies (cm^{-1}) of $K_2Sn_2S_8$, $K_2Sn_2S_5$, $Cs_2Sn_2S_6$, and Cs_2SnS_{14}

$K_2Sn_2S_8$ (I)		$K_2Sn_2S_5$ (IV)		$Cs_2Sn_2S_6$ (V)		Cs_2SnS_{14} (VI)	
IR	Raman	IR	Raman	IR	Raman	IR	mode
485	483				490	490	ν(S–S)
	471				469	441	
363		353	367	360	386		$\nu(Sn–S)_{sym}$
	379	343	346		382	362	
338		334	334	332		327	$\nu(Sn–S)_{asym}$
		320					
298		274	306	298		288	deformation
277			270	264		277	and
262							torsional
236		224	218	239		226	modes
		201					
195		186				202	
160		156		158		176	
				149		150	

the direction of [110] and [1$\bar{1}$0] alternately. The $[SnS_3]_{2n}^{2n-}$ chains are cross-linked by sharing the remaining equatorial S

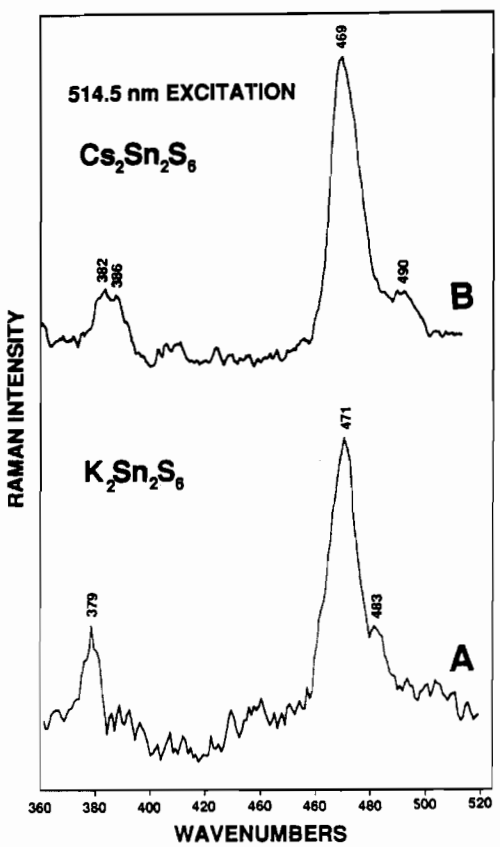

Figure 8. (A) Raman spectrum of $K_2Sn_2S_8$. (B) Raman spectrum of $Cs_2Sn_2S_6$.

atoms of the trigonal bipyramids to form an extended three-dimensional framework. The $(Sn_2S_5)^{2-}$ framework features 1D tunnels running parallel to the *b*-axis. These tunnels contain the K^+ atoms. The K–S distances range from 3.090(5) to 3.640(5) Å with the average of 3.39(21) Å and coordination number of 8.

Structure of $Cs_2Sn_2S_6$ and Its Relationship to $K_2Sn_2S_5$. In view of the snug fit of the K^+ and Tl^+ ions in the $[Sn_2S_5]^{2-}$ framework, we reasoned that Cs^+ will be too large for its tunnels and may drive the system to a different structure type. Indeed, the structure of V is different from but closely related to that of IV. Its chemical formula can be expressed as $Cs_2Sn_2S_4(S_2)$. The two-dimensional structure of V is shown in Figure 5. Selected bond distances and angles are given in Table X. The $[Sn_2S_4(S_2)]^{2-}$ framework contains distorted SnS_5 trigonal bipyramids as building blocks. Similar $[SnS_3]_n^{2n-}$ chains as found in IV formed by trigonal bipyramids sharing two common edges (both contain an axial S

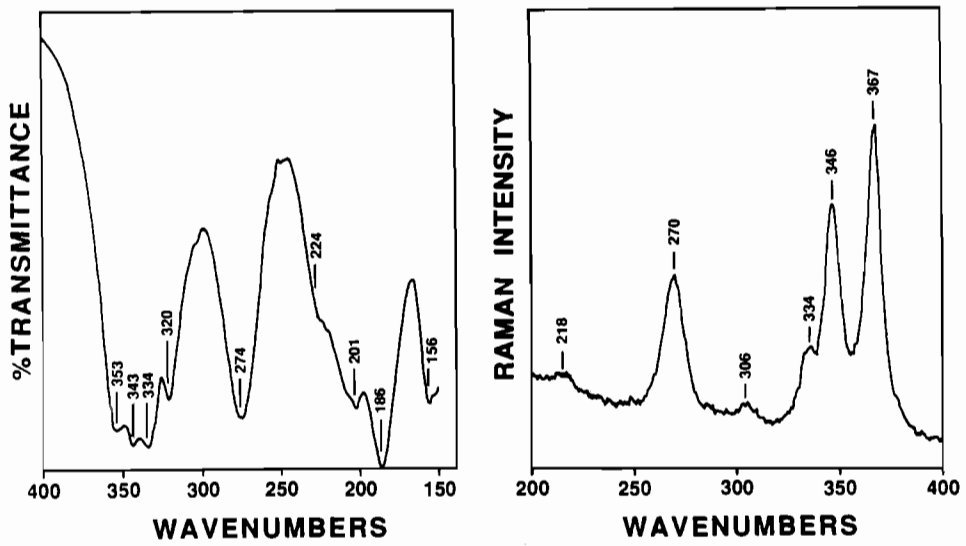

Figure 9. Infrared (A, left) and Raman (B, right) spectra of $K_2Sn_2S_5$.

atom and an equatorial S atom). The $[SnS_3]_n^{2n-}$ chains in V are parallel to the crystallographic *a*-axis and are cross-linked via S–S bonds formed by connecting the remaining equatorial S atoms of the SnS_5 trigonal bipyramids. This gives rise to a two-dimensional structure whose slabs are perforated by large holes. The holes define 14-membered Sn–S rings. The average Sn–S distance in the SnS_5 trigonal bipyramid of V is similar to those in IV, 2.49(9) Å.

The Cs^+ cations are located between the layers. The Cs···S distances range from 3.501(4) to 4.041(3) Å with an average distance of 3.66(17) Å. The coordination number around Cs^+ is 8. The radius of Cs^+ is thus ~0.4 Å larger than that of K^+, which accounts for the fact that the $[Sn_2S_5]^{2-}$ framework is unsuitably small to fit the same number of Cs^+ cations. In order to accommodate Cs^+ the anionic framework responds by substituting the bridging S^{2-} ligands with longer S_2^{2-} ligands, thus increasing the size of the cavities. At the same time, the two sets of parallel $[SnS_2]_n$ chains, which in IV orient along the [110] and [1$\bar{1}$0] directions to form a crisscross pattern, now line up in the same direction, [100] in V. This is shown in Figure 6. In this way, the three-dimensional framework of IV breaks up to form a two-dimensional structure which is more flexible especially in the direction perpendicular to the layers.

Structure of Cs_2SnS_{14}. VI is composed of discrete $[SnS_{14}]^{2-}$ anions and Cs^+ cations. The structure of a single $[SnS_{14}]^{2-}$ anion is shown in Figure 7. The anion features a Sn^{4+} center octahedrally coordinated by two S_4^{2-} and one S_6^{2-} ligands, and thus it is better represented as $[Sn(S_4)_2(S_6)]^{2-}$. The tetraethylammonium salt of the anion has been reported to occur cocrystallized in the same crystallographic site with $[Sn(S_4)_3]^{2-}$.[9] Thus the SnS_6 ring was not well refined. Crystals of VI show no such disorder. Interestingly, analogous compounds were not isolated from the Sn/K_2S_x and Sn/Rb_2S_x systems perhaps due to high solubility in the solvents used during isolation. A related selenium analog, $(Ph_4P)_2Sn(Se_4)_3$,[31,32] is known. Thus far no selenium compound of VI has been prepared. Another tetravalent octahedral metal center chelated with polysulfides is the $[Pt(S_5)_3]^{2-}$ anion.[33,34]

Table XI lists selected bond distances and angles for VI. The average Sn–S distance in V is 2.575(13) Å, which is typical for octahedrally coordinated Sn^{4+} centers.[15] The S–S bond distances are in the normal range from 2.038(8) to 2.074(9) Å, compared to the unreasonably short 1.84(1) Å obtained before from the disordered model.[9] The S–Sn–S angles are in the range between 80.7(2) and 101.6(2)°, which significantly deviate from 90°, the ideal octahedral geometry. This is probably due to the difference in the Sn–polysulfide ring size. The two five-membered SnS_4 rings adopt an envelope shape with S(8) and S(12) sitting outside the SnS_3 planes, respectively. In the seven-membered SnS_6 ring, Sn, S(1), S(3), S(4), and S(6) are lying in the same plane with S(2) and S(5) sitting above or below the plane. A similar conformation is also observed in a seven-membered HgS_6 ring of $[Hg(S_6)_2]^{2-}$.[35] The two Cs^+ cations are surrounded by S atoms with coordination number of 6 for Cs(1) and 7 for Cs(2). The average Cs–S distance is 3.64(7) Å. Interestingly, VI and I are actually synthesized under similar conditions. The size of alkali cation seems to have a dramatic effect on the formation of anions. The layered structure of $[Sn_2S_4(S_4)]^{2-}$ in I cannot accommodate large Cs^+ cations. By a breaking apart into discrete molecular anions like VI, enough room is created for Cs^+.

Vibrational Spectroscopy. The infrared and/or Raman frequencies of $K_2Sn_2S_8$ (I), $K_2Sn_2S_5$ (IV), $Cs_2Sn_2S_6$ (V), and Cs_2SnS_{14} (VI) are listed in Table XII. The IR spectra of α-$Rb_2Sn_2S_8$ (II) and β-$Rb_2Sn_2S_8$ (III) are the same as that of $K_2Sn_2S_8$ (I). We did not measure the Raman spectra of α-$Rb_2Sn_2S_8$ (II) and β-$Rb_2Sn_2S_8$ (III) because they are expected to be similar to $K_2Sn_2S_8$ (I). Since Cs_2SnS_{14} (VI) cannot be isolated in pure form, no Raman spectrum of this compound was measured. The sample used to obtain the IR spectrum was picked by hand from a mixture with $Cs_2Sn_2S_6$.

Representative Raman spectra of $K_2Sn_2S_8$ (I) and $Cs_2Sn_2S_6$ (V) obtained with 514.5-nm excitation are shown in Figure 8. Raman spectra were also obtained with 441- and 488-nm excitations (not shown) but gave similar spectra. In Figure 9A, the mode at 379 cm^{-1} of $K_2Sn_2S_8$ can be assigned to Sn–S stretching vibration by analogy to other tin sulfide complexes.[10-12] The vibrations at 483 and 471 cm^{-1} are assignable to $\nu_{(S-S)sym}$ and $\nu_{(S-S)asym}$, respectively.

Figure 8B shows the Raman spectrum of $Cs_2Sn_2S_6$ with isolated groups of bands assignable to Sn–S stretchings (382 and 386 cm^{-1}), S–S stretching (469 cm^{-1}), and asymmetric stretching (490 cm^{-1}) vibrations. The S–S vibrations are not observed in the IR spectrum of $Cs_2Sn_2S_6$ because the S–S bond is sitting at the center of inversion. For an unbranched polysulfide species of *n* atoms, one may expect $(3n - 3)$ vibrational fundamentals, with $(n - 1)$ skeletal stretching modes, $(n - 3)$ skeletal torsional modes, and $(n - 2)$ skeletal bending modes. The frequencies for the fundamentals fall in the 400–500-cm^{-1} range.[13] The torsional modes are expected at frequencies below 100 cm^{-1} and are difficult to separate from lattice vibrations. Therefore, more exact

(31) Banda, R. M.; Cusick, J.; Scudder, M. L.; Craig, D. C.; Dance, I. G. *Polyhedron* **1989**, *8*, 1999–2001.
(32) Dhingra, S.; Huang, S.-P.; Kanatzidis, M. G. *Polyhedron* **1990**, *11*, 1389–1395.
(33) Wickenden, A. E.; Krause, R. A. *Inorg. Chem.* **1969**, *8*, No. 4, 779–783.
(34) Spangenberg, M.; Bronger, W. *Z. Naturforsch.* **1978**, *33b*, 482–484.
(35) Müller, A.; Schimanski, J.; Schimanski, U. *Angew. Chem., Int. Ed. Engl.* **1984**, *23*, 159–160.

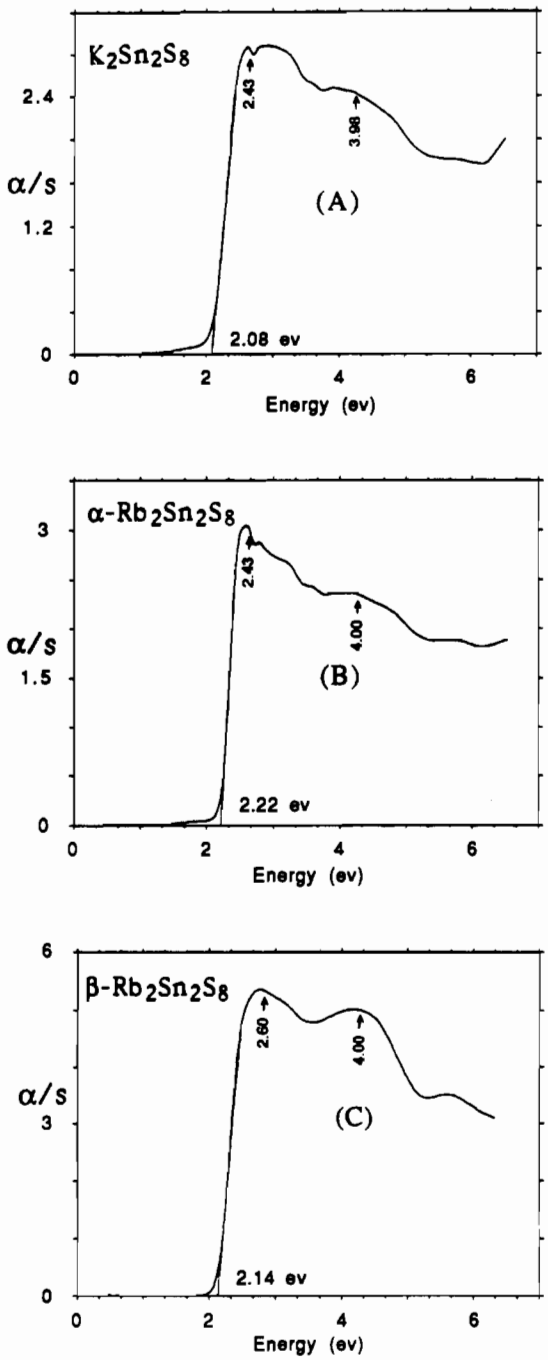

Figure 10. Optical absorption spectra of $K_2Sn_2S_8$, α-$Rb_2Sn_2S_8$, and β-$Rb_2Sn_2S_8$.

assignment of S–S vibrations would require complete polarization data from single-crystal studies.

Figure 9 shows the IR and Raman spectra of $K_2Sn_2S_5$ (IV). The vibrations at 353 and 343 cm^{-1} in the IR and at 367 and 346 cm^{-1} in the Raman spectra are due to $\nu_{(Sn-S)sym}$. The 334- and 320-cm^{-1} (IR) and 334-cm^{-1} modes (Raman) are assignable to $\nu_{(Sn-S)asym}$.

UV/Vis/Near-IR Spectroscopy. The optical properties of $K_2Sn_2S_8$, α-$Rb_2Sn_2S_8$, β-$Rb_2Sn_2S_8$, $K_2Sn_2S_5$, and $Cs_2Sn_2S_6$ were assessed by studying the UV/visible/near-IR reflectance spectra of the materials. The spectra confirm the semiconductor nature by revealing the presence of an optical gap as shown in Figures 10 and 11. The spectra of all compounds clearly exhibit steep absorption edges from which the band-gap can be assessed at an average of 2.15 eV for I–III, 2.36 eV for IV, and 2.44 eV for V. These transitions are probably charge transfer in character from the primarily S-based valence band to the primarily Sn-based conduction band. Other electronic transitions occur at higher

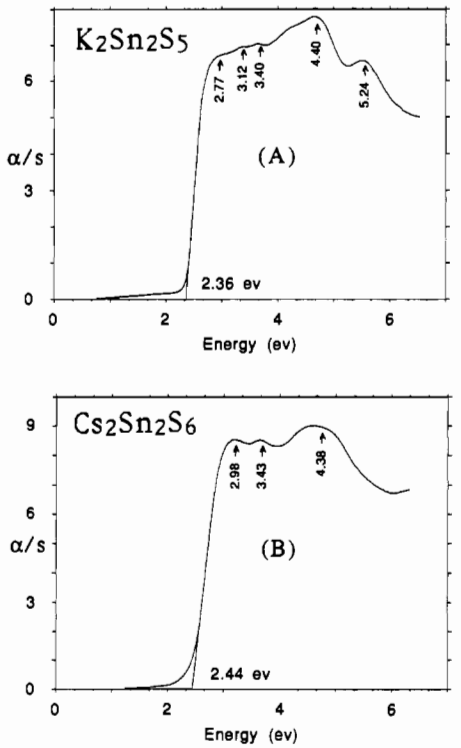

Figure 11. Optical absorption spectra of $K_2Sn_2S_5$ and $Cs_2Sn_2S_6$.

energies, and they are indicated in the spectra in Figures 10 and 11. The smaller band gaps of $K_2Sn_2S_8$, α-$Rb_2Sn_2S_8$, and β-$Rb_2Sn_2S_8$ compared to those of $K_2Sn_2S_5$ and $Cs_2Sn_2S_6$ are consistent with the respective orange and yellow colors of the two groups. By comparison, the corresponding band gap of SnS_2 is 2.16 eV.

Conclusion

The results presented here further illustrate the utility of the molten polychalcogenide salt method to produce a variety of novel solid-state and even molecular structures. $K_2Sn_2S_8$, α-$Rb_2Sn_2S_8$, β-$Rb_2Sn_2S_8$, and $Cs_2Sn_2S_6$ are the first examples of two-dimensional alkali tin–polysulfides and, to our knowledge, first solid-state main group metal–polysulfides. Even though the molten polychalcogenide route allows for a wide range of reaction temperatures, the final products depend on the temperature used. In this system we found lower temperatures (<300 °C) and/or melts with longer polysulfides (A_2S_x, $x > 3$) are generally required to incorporate polysulfides in the anionic framework. We also found higher reaction temperatures promote crystallization of phases containing shorter S_x^{2-} chains and/or monosulfide such as in $Cs_2Sn_2S_6$ and $K_2Sn_2S_5$. Finally, an important factor seriously affecting the structure of the products, in ways not well understood at present, is the size of alkali metal counterion. All compounds exhibit well-defined, abrupt optical gaps associated with S → Sn charge-transfer excitations.

Acknowledgment. Support from the National Science Foundation (Grant DMR-9202428) and the Beckman Foundation is greatly appreciated. C.V. thanks Professor G. T. Babcock for financial support from NIH Grant 71-1247. We also thank Dr. B. R. Vincent at Molecular Structure Corp., The Woodlands, TX, for the X-ray diffraction data collection and structure determination of $K_2Sn_2S_8$.

Supplementary Material Available: Tables of crystal and structural analysis data, calculated and observed X-ray powder diffraction patterns, atomic coordinates of all atoms, and anisotropic and isotropic thermal parameters of all atoms for $K_2Sn_2S_8$, α-$Rb_2Sn_2S_8$, β-$Rb_2Sn_2S_8$, $K_2Sn_2S_5$, Cs_2SnS_{14}, and $Cs_2Sn_2S_6$ (19 pages). Ordering information is given on any current masthead page.